A Compact CMOS 363 GHz Autodyne FMCW Radar with 57 GHz Bandwidth for Dental Imaging

Morteza Tavakoli Taba[1], S. M. Hossein Naghavi[1], Morteza Fayazi[1], Ali Sadeghi[2], M. Aseeri[4], A. Cathelin[3], E. Afshari[1]

[1]University of Michigan, USA, [2]University of Washington, USA, [3]STMicroelectronics, France,[4]KACST, Saudi Arabia

Millimeter-wave and terahertz circuits have numerous applications in radars, remote sensing, and next-generation 5G network. Among the THz radars, frequency-modulated continuous-wave (FMCW) topology has drawn attention for imaging and security applications. Comparing the state-of-the-art FMCW radars [1-3], [6], most wideband radars are implemented with costly SiGe HBT transistors with a f_{max} of ~380 GHz. Transistor scaling increases the f_{max} of low-cost CMOS technologies, which makes them suitable for high-precision imaging applications such as dental imaging that require wide bandwidth, compactness, and high operation frequency.

In this paper, a compact, wideband, and fully integrated CMOS FMCW radar is proposed. A five-stage voltage-controlled ring oscillator (VCRO) is designed, and the fifth harmonic signal is efficiently extracted to achieve wideband and high-frequency signal generation. The radar achieves a 57 GHz tuning range with a peak EIRP of 6.2 dBm and a 5.8 dB power variation, the lowest power fluctuation of reported FMCW radars from the 200-400 GHz range. The radar is further used and tested in a dental imaging setup to capture the teeth cavities and root canals.

Most of the implemented CMOS voltage-controlled oscillators (VCOs) in the literature suffer from limited bandwidth [5], while the HBT counterparts achieve 60-70 GHz bandwidth around 200-300 GHz [1, 6]. The well-known cross-coupled and Colpitts push-push topologies shown in Fig.1 are optimized for maximum BW, achieving a bandwidth and an in-band power variation of 40 and 26.8 GHz, 11 and 8 dB, respectively. High in-band power variation is because lower harmonic generation (e.g., second or third harmonic) requires a large fundamental frequency tuning range resulting in a significant power variation. To alleviate the power variation and limited absolute bandwidth issue, a ring oscillator (RO) capable of producing higher-order harmonics is used. Fig.1 illustrates the maximum oscillation frequency of a RO versus the phase shift of each stage (φ), showing a flat response for N = 3, 5. Here, N = 5 is chosen since a lower fundamental frequency tuning range is required for a given target frequency bandwidth, resulting in lower in-band power variation. Moreover, the lower fundamental frequency of the five-stage VCRO means higher transistor activity and power gain. This is important because the power of fifth and higher-order harmonics generated in CMOS transistors is generally small compared to first to fourth harmonics, but a lower required fundamental frequency can compensate for this effect. Here, designing a 363 GHz VCRO with a 57 GHz tuning range results in an 11.4 GHz tuning range around the fundamental frequency of 72.6 GHz.

Fig.2 shows the circuit schematic of the oscillator. A common-source amplifier with an inductive loading is used to generate high voltage swing at the fundamental frequency and hence higher harmonic power. Simulation results show that the in-band power variation is minimized for gate voltages much smaller than V_{DD}. Thus, a metal-insulator-metal (MIM) capacitor (C_B) with a resistor (R_B) is used to isolate each stage's gate and drain bias. The bias and the width of the transistors are optimized for maximum tuning range. Moreover, a T-type passive phase shifter is utilized to tune the oscillator's output frequency (shown in Fig.2). The passive phase shifter offers a compact area and zero DC power over the active phase shifter. Lowering the capacitance of the varactor inside the phase shifter reduces the phase shift leading to a higher oscillation frequency, given that the total phase shift across the loop is constant. Here, the target frequency is chosen to be 363 GHz since the quality factor of the T-lines (L_d) is higher at the fundamental frequency of 72.6 GHz, improving the output power, compared to a fundamental frequency of 50 GHz targeting an output frequency of 200 GHz. Furthermore, the output of each stage is connected at point X so that the fifth harmonic currents from each stage add constructively. Load pull simulation reveals a low impedance required for the fifth harmonic power matching; therefore, a modified folded slot antenna with an impedance of 35 ohm at 363 GHz is designed. The width of the feeding line and gaps inside the antenna is carefully optimized to achieve small impedance, high antenna gain, and efficiency. A ~λ/4 stub (L_{stub}) is designed as a part of the antenna matching and provides the necessary DC bias of drain voltage for each stage of VCRO. The output power at the antenna port for different harmonics is plotted in Fig.2, showing that the fifth harmonic power is at least 26 dB higher than other harmonics, proving the suppression of undesired harmonics. The power combining network with the antenna is simulated in HFSS at the first and fifth harmonic. It demonstrates the surface current densities flowing to the antenna at the fifth harmonic (Fig.3, bottom right) while the first harmonic current densities cancel at point X (Fig.3, bottom left). Additionally, to increase the antenna's directivity, a 1 cm silicon lens and a 280 μm silicon slab are attached at the back of the chip, as shown in Fig.3.

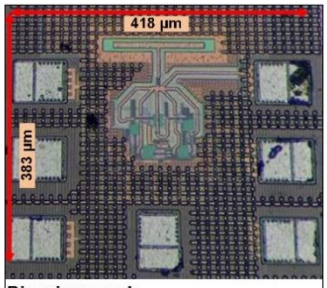

Die micrograph.

To minimize the area of the radar, an autodyne radar topology is selected, meaning that there is a single antenna for radiation, and reception, with the oscillator core transistors acting as the mixer [1]. Fig.2 illustrates the overall mechanism of the receiver. The received signal is summed with the transmitted signal at the antenna port. The TX+RX signals appear at the gate of each stage of VCRO and are mixed by the second-order nonlinearity of the MOS transistors to generate the IF signal as shown in Fig.3. The IF signal is extracted from the V_{DD} line using a bias-T and further amplified and processed.

Fig.4 illustrates the radar's measurement setup. The FMCW radar is characterized by an FSW Rohde&Schwarz spectrum analyzer and an FS-Z500 harmonic mixer. The total radiated output power is measured using a VDI Erikson PM4 power meter and a WR-10 horn antenna. The radar achieves a 57 GHz (338.4-395.4 GHz) bandwidth and a peak EIRP of 6.2 dBm with 5.8 dB variation across the tuning range shown in Fig.4. Fig.4 also illustrates the far-field distance of the radar, which starts at 15 cm. The antenna radiation pattern in E- and H-plane are plotted for three different frequencies showing a consistent pattern over the tuning range. Range resolution and range accuracy measurement setups are shown in Fig.5. The measured range accuracy using the phase processing method is 19.8 μm, with ±2σ error (95% confidence) achieved by 100 times averaging. The range resolution results are shown in Fig. 5 (top right), illustrating the ability of the radar to resolve objects that are 2.63 mm apart following the conventional range resolution equation $\Delta R = c/(2\times BW)$. Moreover, to show the imaging capability of the radar, an image of the human's teeth is shown in Fig.5. Unlike [4], the radar successfully detects the cavities and canals inside the teeth thanks to the high special resolution of the radar (λ/2 = 400 μm). Fig.6 illustrates the comparison of our work to the state-of-the-art FMCW radars. Compared to the other reported CMOS radars, this radar achieves the highest tuning range without additional off-chip sources [3], comparable performance to HBT counterparts [1, 6]. Note that, only CMOS transistors are used in our design.

References:

[1] S. M. Hossein Naghavi et al., "22.4 A 250GHz Autodyne FMCW Radar in 55nm BiCMOS with Micrometer Range Resolution," ISSCC, 2021.

[2] A. Visweswaran et al., "9.4 A 145GHz FMCW-Radar Transceiver in 28nm CMOS," ISSCC, 2019.

[3] X. Yi et al., "4.8 A Terahertz FMCW Comb Radar in 65nm CMOS with 100GHz Bandwidth," ISSCC, 2020.

[4] C. Jiang et al., "25.5 A 320GHz subharmonic-mixing coherent imager in 0.13μm SiGe BiCMOS," ISSCC, 2016.

[5] H. Koo et al., "Design and Analysis of 239 GHz CMOS Push-Push Transformer-Based VCO With High Efficiency and Wide Tuning Range," TCAS, July 2015.

[6] J. Al-Eryani et al., "Fully Integrated Single-Chip 305–375-GHz Transceiver With On-Chip Antennas in SiGe BiCMOS," Trans.THz, 2018.

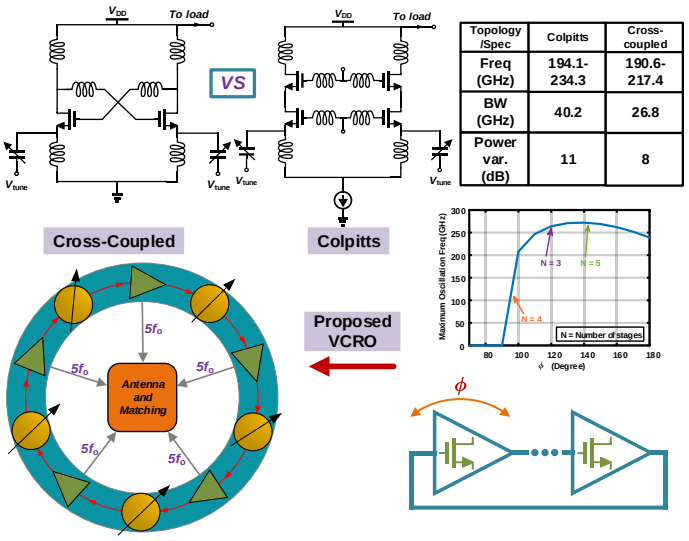

Topology /Spec	Colpitts	Cross-coupled
Freq (GHz)	194.1-234.3	190.6-217.4
BW (GHz)	40.2	26.8
Power var. (dB)	11	8

Fig. 1. Comparison of maximum achievable bandwidth of two push-push VCOs, maximum oscillation frequency of RO, block diagram of the VCRO.

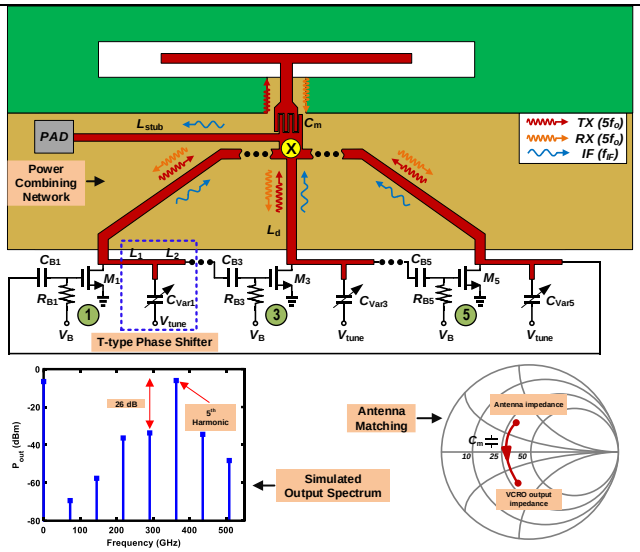

Fig. 2. Circuit diagram of the VCRO including the receiver mechanism, the simulated output power spectrum of the VCRO at the antenna port, and the antenna matching.

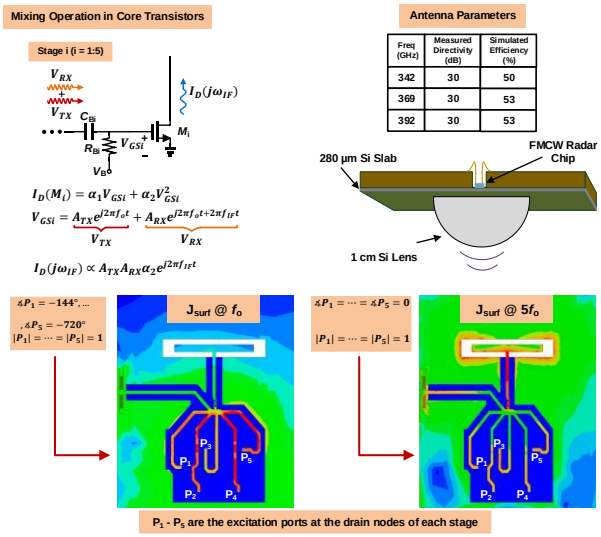

Freq (GHz)	Measured Directivity (dB)	Simulated Efficiency (%)
342	30	50
369	30	53
392	30	53

Fig. 3. Detail of mixing operation of receiver; directivity calculated from the antenna pattern measurements; simulated surface current density at f_o and $5f_o$ (excitation port locations are shown).

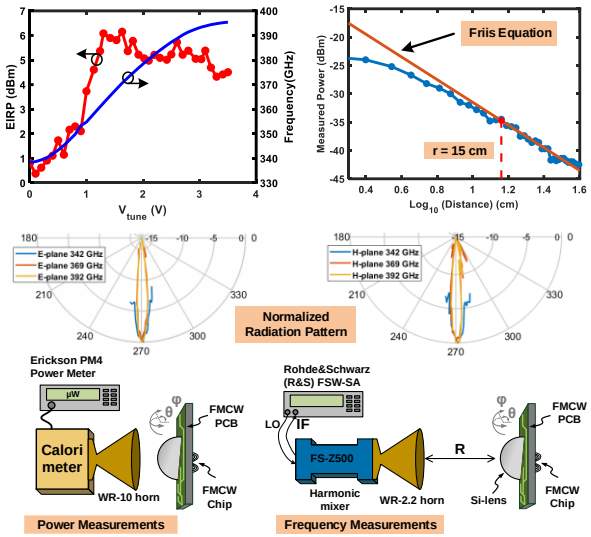

Fig. 4. Measured Far field, measured EIRP and tuning range, E- and H- plane patterns, and their respective measurement setups.

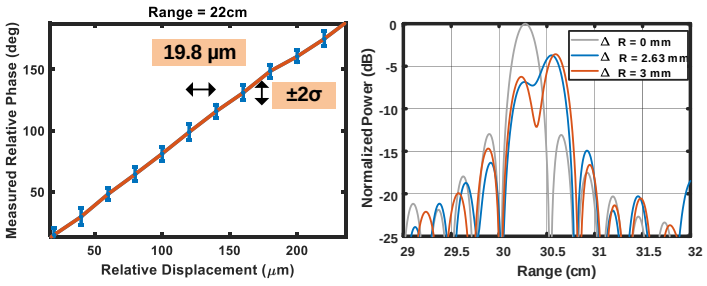

Range (cm)	Range acc. W/ 100 avg. (k =2)
22	19.8 μm
36	20.8 μm
57	41.6 μm

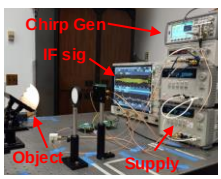

Fig. 5. Measured phase resolution and range accuracy and their respective measurement setups.

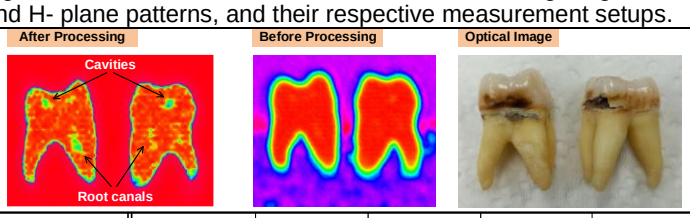

Ref.	This Work	ISSCC 2021 [1]	ISSCC 2019 [2]	ISSCC 2020 [3]	Trans. THz [6]
Frequency (GHz)	338.4-395.4	191-257.7	138-151	220-320	305-375
Frequency Tuning (GHz/%)	57/15.5	66.7/29.7	13/9	100/37	70/20.6
f_{max} (GHz)	290	340	NA	280	370
Peak EIRP (dBm)	6.2	17	11.5	0.6,20****	6,18.4****
EIRP Fluctuation (dB)	5.8	6.5	1.5	8.8	10.5
Range Resolution (mm)	2.63**	0.054/0.167	11.5	1.5	2.1
DC Power (mW)	152	68	500	850	1700
Technology	55 nm BiCMOS***	55 nm BiCMOS	28 nm CMOS	65 nm CMOS	130 nm BiCMOS
Area (mm^2)	0.16	0.22	6.5	5	2.85

* f_{max} of CMOS transistors
** After 100 times averaging of the data.
*** Only MOS transistors are used.
**** A TPS lens is used.

Fig. 6. Comparison table and the human teeth image before and after processing with the detected cavities and root canals.